Hydrodynamics of Upflow Anaerobic Sludge Blanket Reactors

Ting-Ting Ren, Yang Mu, Bing-Jie Ni, and Han-Qing Yu
Dept. of Chemistry, University of Science and Technology of China, Hefei 230026, China

DOI 10.1002/aic.11667
Published online December 23, 2008 in Wiley InterScience (www.interscience.wiley.com).

The hydrodynamic characteristics of upflow anaerobic sludge blanket (UASB) reactors were investigated in this study. A UASB reactor was visualized as being set-up of a number of continuously stirred tank reactors (CSTRs) in series. An increasing-sized CSTRs (ISC) model was developed to describe the hydrodynamics of such a bioreactor. The gradually increasing tank size in the ISC model implies that the dispersion coefficient decreased along the axial of the UASB reactor and that its hydrodynamic behavior was basically dispersion-controlled. Experimental results from both laboratory-scale H_2-producing and full-scale CH_4-producing UASB reactors were used to validate this model. Simulation results demonstrate that the ISC model was better than the other models in describing the hydrodynamics of the UASB reactors. Moreover, a three-dimensional computational fluid dynamics (CFD) simulation was performed with an Eulerian-Eulerian three-phase-fluid approach to visualize the phase holdup and to explore the flow patterns in UASB reactors. The results from the CFD simulation were comparable with those of the ISC model predictions in terms of the flow patterns and dead zone fractions. The simulation results about the flow field further confirm the discontinuity in the mixing behaviors throughout a UASB reactor. © 2008 American Institute of Chemical Engineers *AIChE J,* 55: 516–528, 2009

Keywords: computational fluid dynamics, dispersion, Eulerian-Eulerian, hydrodynamics, model, upflow anaerobic sludge blanket

Introduction

The upflow anaerobic sludge blanket (UASB) reactor has been the most widely used high-rate anaerobic reactor for wastewater treatment throughout the world since 1980s. Its treatment capacity depends on the amount of active biomass retained, as well as the contact between biomass and wastewater. Performance of a UASB reactor, in terms of chemical oxygen demand (COD) removal and energy yield, is usually governed by two main interrelated factors: microbiological processes and hydrodynamics. Thus, investigation into the reactor hydrodynamics is highly desirable.[1] Previous studies on the UASB hydrodynamics have shown that they could be well described by the multi-CSTR (continuous stirred tank reactor) model,[2–5] in which the equal-sized CSTRs (ESC) model is commonly used. Typically, in such a model a number of tanks in series (N) and mean residence time are employed to describe the deviations from the ideal CSTR or the plug-flow reactor (PFR). The number of tanks in the ESC model, N, can be calculated from the following equation[6]:

$$N = \frac{1}{\sigma_\theta^2} \tag{1}$$

where σ_θ^2 is the variance of the dimensionless residence time distribution. The N value calculated from Eq. 1 is an important criterion to judge the flow patterns in reactor. Generally, $N = 1$ represents a completely mixed flow, whereas $N = \infty$ means a plug-flow. Integration of a simple dynamic mass balance around the strand of reactors generates the residence

Correspondence concerning this article should be addressed to H.-Q. Yu at hqyu@ustc.edu.cn.

time distribution (RTD) of the system. The concentration of a tracer in the Nth reactor is given in Eq. 2, where θ is defined as dimensionless time, i.e., the Erlang distribution.[7]

$$E(\theta) = \frac{N^N}{(N-1)!}\theta^{N-1}e^{-N\theta} \tag{2}$$

Conceptually, this model has a precise definition of the inlet and outlet boundary conditions. However, the ESC model is based on the equal-sized tanks series and is not related with whether the parameter N is an integer or not. In this case, the dispersion coefficient in a bioreactor is assumed to be uniform. On the other hand, the dispersion coefficients actually vary at the different heights of a UASB reactor and considerably increase near the sludge bed bottom.[8–12] Because the superficial liquid velocity is often lower than 1 m h^{-1} in a UASB reactor, the distribution of substrate and intermediates along the reactor height is far from uniform.[13] Thus, the dispersion should decrease along the axis of a UASB reactor from the bottom to the top, implying that the size of tanks in the multi-CSTRs model should stepwise increase.

Because of its complex nature, the local hydrodynamic behavior of UASB reactors is not well documented yet. Thus, an in-depth investigation and elucidation of the flow patterns in a UASB reactor are desirable. A hydrodynamic model composed of a hydraulic model for analyzing dispersion and computational fluid dynamic (CFD) model for flow patterns and phase holdup visualization should be established.

The CFD method has been demonstrated to be a useful tool for understanding flow behaviors and can be used to replace the time-consuming and expensive experiments to a large extent.[14] Two main approaches exist, i.e., the Eulerian approach, which regards the dispersed phases as interpenetrating continua, and the Lagrangian approach, which treats the dispersed phases as discrete entities.[15–17] With the two approaches the same results can be obtained if adequate numerical methods are used to solve the resulting equations.[18] However, since in the Lagrangian approach tremendous computational efforts will be needed to track each single gas bubble and/or solid particle, it is mainly used in dilute systems.[19]

Vesvikar and Al-Dahhan[20] performed a three-dimensional (3-D) steady-state CFD simulation for mimic anaerobic reactors to visualize the flow patterns and estimated the hydrodynamic parameters. Wu and Chen[21] introduced the non-Newtonian fluid theory into the CFD model for anaerobic reactor simulations. However, most relevant studies are focused on single- or two-phase flows. Information about the modeling of three-phase (gas–liquid–solid) flows in a UASB reactor is still very limited.

Therefore, the present work was aimed at developing hydraulic and CFD models to describe the hydrodynamics of UASB reactors. An increasing-sized CSTRs (ISC) model was established to describe the dispersion feature of the UASB reactor. Experimental results from both laboratory-scale H_2-producing and full-scale CH_4-producting UASB reactors were employed to validate the established mode. Moreover, a 3-D unsteady CFD model simulation was performed to visualize the phase holdup and flow patterns in the reactors.

Model Development

Hydraulic model

Extended Equal-Sized CSTRs (EESC) Model. The schematic diagram of the ESC model is shown in Figure 1a. If the tanks in series model are merely regarded as a residence time distribution function, whose form depends solely on the N value, it becomes possible to sort out the quantization problem in the analysis of high-dispersion systems. An introduction of a noninteger number of hypothetical tanks in series will yield the desired results. The exit age distribution of the extended equal-sized CSTRs (EESC) model (shown in Figure 1b) is given by a subset of the gamma distribution family[6]:

$$E(\theta) = \frac{N^N}{\Gamma(N)}\theta^{N-1}e^{-N\theta} \tag{3}$$

When N is an integer, it is identically equal to the Erlang distribution (Eq. 2). The EESC model sorts out the quantization problem, as N tends to 1 in the multi-CSTRs model.

Establishment of an Increasing-Sized CSTRs Model. The UASB reactor is visualized as being set-up of a number of gradually increasing-sized CSTR tanks (Figure 1c). The initial concentration C_0 in the first tank (V_1) at $t = 0$ is described by Eq. 4:

$$C_0 = \frac{M}{V_1} \tag{4}$$

The tracer mass (M) balance at the inlet and outlet of each tank is described as follows:

For the 1st CSTR:

$$V_1\frac{dC_1}{dt} + QC_1 = 0 \tag{5}$$

Integration of Eq. 5 gives the following equation for the tracer concentration in the first tank:

$$C_1 = C_0\exp\left(-\frac{t}{T_1}\right) \tag{6}$$

where T_1 is the mean residence time in the first tank and Q is the influent flow rate.

For the 2nd CSTR:

$$V_2\frac{dC_2}{dt} + QC_2 = QC_1 = QC_0\exp\left(-\frac{t}{T_1}\right) \tag{7}$$

Integration of Eq. 7 results in the following equation for the tracer concentration in the second tank:

$$C_2 = \frac{C_0T_1}{T_2 - T_1}\left[\exp\left(-\frac{t}{T_2}\right) - \exp\left(-\frac{t}{T_1}\right)\right] \tag{8}$$

The following equation can be obtained for the Nth CSTR using mathematic induction:

$$C_N = C_0T_1\sum_{i=1}^{N}\left[\frac{T_i^{N-2}}{\prod_{j=1,j\neq i}^{N}(T_i - T_j)}\mathrm{e}^{-\frac{1}{T_i}t}\right] \tag{9}$$

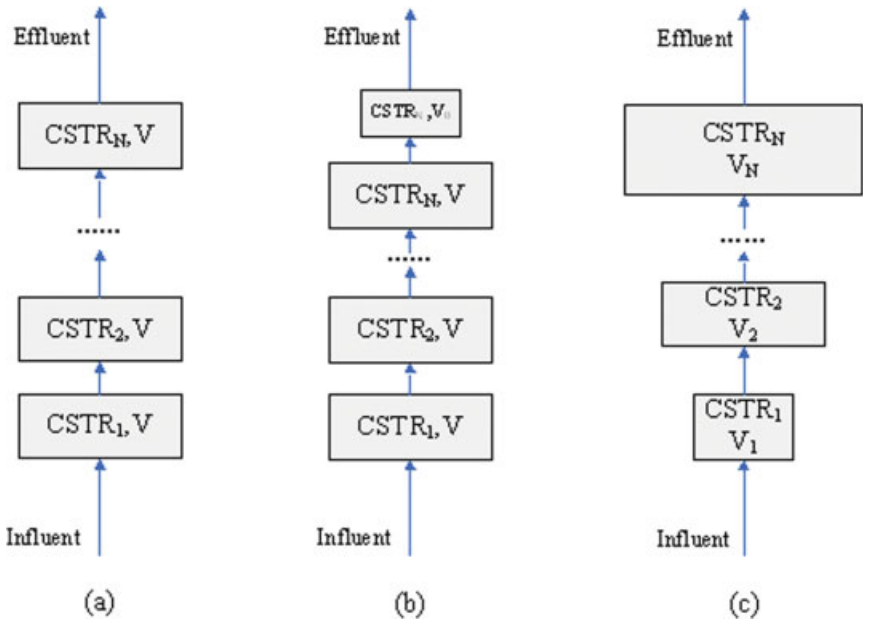

Figure 1. A schematic diagram of the model: (a) ESC model; (b) EESC model; and (c) ISC model.

[Color figure can be viewed in the online issue, which is available at www.interscience.wiley.com.]

The exit age distribution function E(t) is defined as follows:

$$E(t) = \frac{Q}{M} C_N \tag{10}$$

In Eq. 9, $T_i = V_i/Q$. Substitution of Eqs. 4 and 9 into Eq. 10 yields:

$$E(t) = \sum_{i=1}^{N} \left[\frac{T_i^{N-2}}{\prod_{j=1, j\neq i}^{N} (T_i - T_j)} \mathrm{e}^{-\frac{1}{T_i}t} \right] \tag{11}$$

Setting $V_1 = r_1 V_{\mathrm{tot}}$, $V_2 = r_2 V_{\mathrm{tot}}$, ..., $V_N = r_N V_{\mathrm{tot}}$, where V_N is the volume of the Nth tank, V_{tot} is the total volume of all tanks, and r_N is the fraction coefficient. The resulting dimensionless form of Eq. 11 is as follows:

$$E(\theta) = \bar{t} \times E(t) = \frac{Q}{V_{\mathrm{tot}}} \sum_{i=1}^{N} \left[\frac{r_i^{N-2}}{\prod_{j=1, j\neq i}^{N} (r_i - r_j)} \mathrm{e}^{-\frac{\theta}{r_i}} \right] \tag{12}$$

Then, the governing equations for the ISC model can be written as follows:

$$\begin{cases} E(\theta) = \dfrac{Q}{V_{\mathrm{tot}}} \displaystyle\sum_{i=1}^{N} \left[\dfrac{r_i^{N-2}}{\prod_{j=1, j\neq i}^{N} (r_i - r_j)} \mathrm{e}^{-\frac{\theta}{r_i}} \right] \\ r_1 + r_2 + \cdots + r_N = 1 \\ \dfrac{r_N}{r_{N-1}} > 1 \end{cases} \tag{13}$$

To establish the mass balance equation of tracer in series of mixed reactor compartments, the water and tracer loadings at the point proceeding of Nth compartment are described in Eq. 14:

$$I_{\mathrm{in},N} = Q_{\mathrm{in}} C_{N-1} \tag{14}$$

The UASB reactor could be divided into three compartments: a sludge bed and a sludge blanket, both are mixed with respect to the liquid phase, and a plug flow region to describe the internal settler.[4] In the present work, a similar approach is adopted and the settler compartment is assumed as a subsequent plug flow reactor to the ISC model in series.

Parameter Estimation. As most of the model parameters in the ISC models cannot be measured, they have to be estimated through minimizing the sum of the squared difference χ^2 between the measured (C^{exp}) and calculated (C^{cal}) values of the tracer concentrations at the sampling ports over sampling times (N_{time}), i.e., the following function is minimized:

$$\chi^2 = \sum_{i=1}^{N_{\mathrm{time}}} \left(\frac{C_i^{\mathrm{cal}}(p) - C_i^{\mathrm{exp}}}{\sigma_i^{\mathrm{exp}}} \right)^2 \tag{15}$$

Software AQUASIM 2.0 is used to estimate the model parameters.[22]

CFD model

Eulerian-Eulerian Model. A 3-D transient CFD model is used to simulate the hydrodynamics of the three-phase (gas–liquid–solid) UASB reactor. In the CFD simulation, a multiphase control volume, composed of one continuous (wastewater) and two dispersed phases (gas bubbles and microbial granules), is analyzed with the Eulerian-Eulerian model. This model is chosen because of the large number of particles.[23] Each phase is assumed to be incompressible in this study.

The wastewater is regarded as pure water at 37°C. The sludge takes up about 50% of the volume in sludge bed region and is considered to be spherical solid granules with a density of 1070 kg m^{-3}, diameter of 2 mm, and dynamic viscosity of 5 mPa s. These media values could be appraised as an approximation of the physical properties of the anaerobic granules observed in UASB reactors.[24] The gas bubbles have a density of 1.139 kg m^{-3} and a dynamic viscosity of 0.019 mPa s. The gas phase volume fraction is related to the gas production and the gas bubbles have a diameter of 0.1 mm.

Governing Equations. The mass and momentum conservation equations are solved in a computational 3-D mesh. The phase volume fractions comply with the compatibility conditions:

$$\sum_{k=1}^{n} \alpha_k = 1 \tag{16}$$

The conservation equations of mass and momentum for each phase in the Eulerian-Eulerian formulation are defined as follows:

$$\nabla \cdot (\rho_k \alpha_k \vec{u}_k) = 0 \tag{17}$$

$$\nabla \cdot (\alpha_k(\rho_k \vec{u}_k \vec{u}_k)) = \nabla \cdot (\mu_{\text{eff,k}} \alpha_k (\nabla \vec{u}_k + (\nabla \vec{u}_k)^T)) - \alpha_k \nabla p + \overrightarrow{M}_{I,k} \tag{18}$$

Where subscript k denotes the physical quantity related to phase k, α_k denotes the volume fraction of phase k. μ_{eff} is the effective viscosity accounting for turbulence, and P is the pressure. $\vec{M}_{I,k}$ represents the total interfacial momentum between the dispersed phase and the continuous phase, and is formed by the sum of the interfacial forces attributed to the drag, the lift, the virtual mass force, and the turbulent dispersion force.

Interphase Momentum Transfer. In this study, only drag forces and lift forces between the continuous phase and the dispersed phase are considered. The drag forces exerted by the dispersed phase on the continuous phase are calculated as:

$$M_{\text{D,lg}} = \frac{3}{4}\frac{C_{\text{D,lg}}}{d_{\text{g}}}\rho_l \alpha_{\text{g}} |u_{\text{g}} - u_{\text{l}}| (u_{\text{g}} - u_{\text{l}}) \tag{19}$$

$$M_{\text{D,ls}} = \frac{3}{4}\frac{C_{\text{D,ls}}}{d_{\text{s}}}\rho_{\text{l}} \alpha_{\text{s}} |u_{\text{s}} - u_{\text{l}}| (u_{\text{s}} - u_{\text{l}}) \tag{20}$$

where C_{D} is the drag coefficient and d is the diameter.

As the volume fraction of gas is low, the bubbles are assumed as spheres and the Schiller and Naumann drag model could be used to calculate the drag forces.[23] The drag coefficient exerted by the gas phase on the liquid phase, $C_{\text{D,lg}}$, is obtained as follows:

$$C_{\text{D,lg}} = \begin{cases} \dfrac{24(1 + 0.15(1-\alpha_{\text{g}})\text{Re}^{0.687})}{(1-\alpha_{\text{g}})\text{Re}} (1-\alpha_{\text{g}})^{-2.65} & (1-\alpha_{\text{g}})\text{Re} \le 1000 \\ 0.44 & (1-\alpha_{\text{g}})\text{Re} > 1000 \end{cases} \tag{21}$$

Where Re is the relative Reynolds number, which is obtained from:

$$\text{Re} = \frac{\rho_{\text{l}} d_{\text{g}} |\vec{u}_{\text{g}} - \vec{u}_{\text{l}}|}{\mu_{\text{l}}} \tag{22}$$

The drag coefficient exerted by the solid phase on the liquid phase, $C_{\text{D,ls}}$, is calculated from the Wen and Yu drag model[23]:

$$C_{\text{D,ls}} = \frac{24}{\alpha_{\text{s}}\text{Re}} \left[1 + 0.15(\alpha_{\text{s}}\text{Re})^{0.687}\right] \alpha_{\text{s}}^{-0.265} \tag{23}$$

The relative Reynolds number for the liquid phase and the solid phase is estimated from the following:

$$\text{Re} = \frac{\rho_{\text{l}} d_{\text{s}} |\vec{u}_{\text{s}} - \vec{u}_{\text{l}}|}{\mu_l} \tag{24}$$

The lift force acting perpendicular to the direction of the relative motion of the two phases is given by:

$$M_{\text{L,lg}} = C_{\text{L}} \rho_{\text{l}} \alpha_{\text{g}} (u_{\text{g}} - u_{\text{l}}) \times (\nabla \times u_l) \tag{25}$$

$$M_{\text{L,ls}} = C_{\text{L}} \rho_{\text{l}} \alpha_{\text{s}} (u_{\text{s}} - u_{\text{l}}) \times (\nabla \times u_l) \tag{26}$$

where C_{L} is the lift coefficient and has a value of 0.5.

The interphase momentum transfer between the two dispersed phases, as well as virtual mass force and turbulent dispersion force between the continuous phase and the dispersed phases are all neglected in this study. If these forces were taken into account, the complexity of numerical computation would significantly increase, but it is not expected to contribute to a better understanding of the system. The effects of the bubble–bubble and solid–solid interactions are, respectively, considered in the calculation of the drag coefficients between the continuous and dispersed phases.

Turbulence Modeling of the Continuous Phase. The turbulence modeling of the continuous phase is based on the two-equation (k, ε) turbulence model derived in a three-phase flow, including the interfacial transfer of turbulent kinetic energy and its dissipation rate. The eddy viscosity model is used to calculate the averaged fluctuating quantities. The Reynolds stress tensor for the continuous phase has the following form:

$$\bar{\bar{\tau}} = -\frac{2}{3}(\rho_{\text{l}} k_{\text{l}} + \rho_{\text{l}} \mu_{\text{t,l}} \nabla \vec{u}_{\text{l}}) \bar{\bar{I}} + \rho_{\text{l}} \mu_{\text{t,l}} \left(\nabla \vec{u}_{\text{l}} + (\nabla \vec{u}_{\text{l}})^T\right) \tag{27}$$

The turbulent viscosity $\mu_{\text{t,l}}$ is written in terms of the turbulent kinetic energy of the liquid phase:

$$\mu_{t,l} = \rho_l C_\mu \frac{k_l^2}{\varepsilon_l} \tag{28}$$

The k_L transport equation in the liquid phase is expressed as:

$$\frac{\partial}{\partial t}(\alpha_l \rho_l k_l) + \nabla(\alpha_l \rho_l k_l \vec{u}_l) = \nabla \cdot \left(\alpha_l \frac{\mu_{t,l}}{\sigma_k} \nabla k_l\right) + \alpha_l G_{k,l} - \alpha_l \rho_l \varepsilon_l + \alpha_l \rho_l \Pi_{k,l} \tag{29}$$

The transport equation of the dissipation rate of ε_L in the liquid phase is expressed as:

$$\frac{\partial}{\partial t}(\alpha_l \rho_l \varepsilon_l) + \nabla(\alpha_l \rho_l \varepsilon_l \vec{u}_l) = \nabla \cdot \left(\alpha_l \frac{\mu_{t,l}}{\sigma_\varepsilon} \nabla \varepsilon_l\right) + \alpha_l \frac{\varepsilon_l}{k_l}\left(C_{1,\varepsilon} G_{k,l} - C_{2,\varepsilon} \rho_l \varepsilon_l\right) + \alpha_l \rho_l \Pi_{\varepsilon,l} \tag{30}$$

where $\Pi_{k,l}$ and $\Pi_{\varepsilon,l}$ represent the influence of the dispersed phases on the continuous phase, and $C_{k,l}$ is the production of the turbulent kinetic energy; σ_k and σ_ε are the turbulent Prandtl numbers for k and ε, respectively; $C_{1,\varepsilon}$ and $C_{2,\varepsilon}$ are constants.

The term $\Pi_{k,l}$ can be derived from the instantaneous equation of the continuous phase and has the following form:

$$\prod_{k,l} = \sum_{p=1}^{2} \frac{k_{pl}}{\alpha_l \rho_l}\left(k_{pl} - 2k_l + \vec{u}_{pl} \cdot \vec{u}_{dr}\right) \tag{31}$$

where k_{pl} is the covariance of the velocities of the continuous phase and the dispersed phase p, $\vec{u}_{pl}$ is the relative velocity, and $\vec{u}_{dr}$ is the drift velocity.

Thus, the $\Pi_{\varepsilon,l}$ is calculated as follows:

$$\prod_{\varepsilon,l} = C_{3,\varepsilon} \frac{\varepsilon_l}{k_l} \Pi_{k,l} \tag{32}$$

The values of the model constants are the standard ones: $C_{1,\varepsilon} = 1.44$, $C_{2,\varepsilon} = 1.92$, $C_{3,\varepsilon} = 1.2$, $C_\mu = 0.09$, $\sigma_k = 1.0$, $\sigma_\varepsilon = 1.3$.

Numerical Solution. The finite volume method is used as the numerical technique. The momentum and continuity equations are discretized using finite volumes. The geometry and the meshes are generated with the preprocessor GAMBIT 2.2. Commercial code Fluent 6.2 is used to solve the continuity and momentum equations. The pressure-velocity coupling is obtained using the Phase Couple SIMPLE (PC-SIMPLE) algorithm.

Experimental

Laboratory-scale H_2-producing UASB reactor

The H_2-producing experiments were carried out in a 7.5 l Plexiglas UASB reactor with an internal diameter of 10 cm and a height of 88 cm (Figure 2). The reactor had a working volume of 4.0 l and was operated at 37 ± 1°C.

This UASB reactor was seeded with CH_4-producing sludge taken from a full-scale anaerobic reactor treating citrate-producing wastewater. It was shifted to an acidogenic reactor for H_2 production by gradually lowering the mixed liquor pH. The pH and volatile suspended solids (VSS) of the seed sludge were 7.1 and 6.3 g l^{-1}, respectively, and the sludge was seeded into the UASB reactor with a sludge concentration of 20.0 g-VSS l^{-1} after thickening. A synthetic sucrose-rich wastewater with a COD level of 9900 mg l^{-1} was used as substrate and was supplemented with buffering chemicals and a sufficient amount of inorganic nutrients as reported previously.[24] The detailed information about the start-up and steady-state performance of this H_2-producing UASB reactor could be found elsewhere.[25]

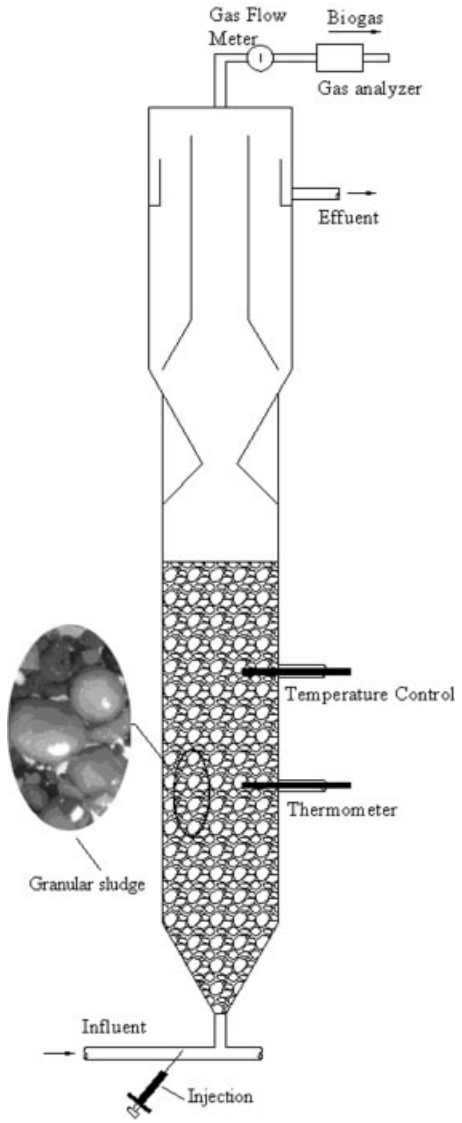

Figure 2. A schematic diagram of the laboratory-scale H_2-producing UASB reactor and pulse injection.

Tracer tests

For the tracer test, a pulse injection of tracer Li^+ was performed at time $t = 0$ in the input stream of the reactor, and the tracer concentrations at time series were measured at the outlet. A solution containing 594 mg Li_2SO_4 (75 mg Li^+) was applied in each tracer run, producing an average Li^+

Table 1. Operating Conditions for the Laboratory-Scale H_2-Producing UASB Reactor

HRT (h)	Flow Rate (l h^{-1})	u_g (m h^{-1})	u_l (m h^{-1})	COD loading (g l^{-1} day^{-1})
4.3	0.93	0.411	0.118	55.8
8.0	0.50	0.271	0.064	30.0
16.3	0.25	0.059	0.031	14.7
26.4	0.15	0.049	0.019	9.0

concentration of 10 mg l^{-1} in the reactor. Experiments were carried out at four different hydraulic retention times (HRTs) as shown in Table 1. Samples were taken every 2 h for an HRT of 26.4 h and every 1 h for an HRT of 16.3 h, and every 0.5 h for an HRT of 8.0 and 4.3 h, respectively. A peristaltic pump (Longer Co., China) was used to control the flow rate. The effluent samples were taken in each tracer test and analyzed. The lithium concentration was determined using flame emission spectroscopy (Vario 6, Analytik Jena AG, Jena, Germany) at a wavelength over 670.8 nm according to the Standard Methods.[26]

Results

Laboratory-scale H_2-producing UASB reactor

The estimated parameters in the ISC model are shown in Table 2. The effective volumes are 5.9 and 6.7 l at an HRT of 8.0 and 4.3 h, respectively, whereas an actual volume is 7.5 l. This indicates that the loss of effective volume is attributed to the granular sludge, bypass flows, and high dispersion within the UASB reactor. For comparison, the results of the EESC model are also displayed in Table 2. The N values in the EESC model calculated from the experimental data using Eq. 1 are 1.9, 1.7, 2.1, and 2.1 for an HRT of 26.4, 16.3, 8.0, and 4.0 h, respectively. Comparison of the final χ^2 values suggests that the EESC model simulation is not as accurate as the ISC model.

For the parameter estimation of the ISC model, there is a good agreement between the measured and calculated tracer trajectories (Figure 3). However, the EESC model is not effective to describe the reactor hydrodynamics. This further demonstrates that the dispersion nonuniformity is the most important factor governing the hydrodynamic characteristics of the UASB reactor.

If the Monod or first-order kinetics dominate, a plug-flow reactor can be more effective. However, the flow pattern of this UASB reactor is not near to plug-flow, because the N value calculated from Eq. 1 is only around 2 at four HRTs (Table 2). This result is different from those of previous studies.[9,27] Generally, mixing in a continuously flow reactor with three phases (gas–liquid–solid), such as the UASB, will mainly depend on the superficial liquid velocity, superficial gas velocity, phase physical properties, phase hold-up, and reactor geometry.[24,28,29] In the present work, both superficial gas and liquid velocities vary simultaneously (Table 1), and their effects overlap with each other. Therefore, the flow patterns should be different for different reactors and operating conditions.

Full-scale CH_4-producing UASB reactor

The hydrodynamics of a laboratory-scale H_2-producing UASB reactor is studied experimentally in this work. However, the hydrodynamics of a full-scale UASB reactor could be completely different from those of laboratory-scale UASB reactor in terms of superficial liquid velocity, accumulating superficial gas velocity, and sudden release of enclosed biogas bubbles in the sludge bed.

The experimental results reported by Batstone et al.[27] are used to validate our model here. This reactor was a full-scale CH_4-producing UASB with a 1400 m^3 working volume and was fed with slaughterhouse wastewater with a COD of 5 g l^{-1} at an HRT of 24 h. Accordingly, the average loading rate was 2.7 g-COD l^{-1} day^{-1}.

The simulated results of this full-scale reactor using our ISC model are shown in Figure 4. The parameter N in the ISC model is calculated to be 4, and the volume ratio of the four tanks is 1:1.5:20:210. The final χ^2 value in the ISC model is estimated to be 2.6. Comparatively, χ^2 is 4.4 in the 1:15 two-tank model and 28.8 in the 1:1 two-tank model, respectively.[27] This shows that the ISC model is also applicable to describing the hydrodynamics of a full-scale CH_4-producing UASB reactor.

Mixing characteristics of a UASB reactor

It is anticipated that there is a discontinuity in the mixing behavior throughout a UASB reactor, which could be verified by the ISC model. The experimental results reported by Lou et al.[30] are used to validate this model. Their experiments were carried out with a 10.4-l UASB reactor. The three sampling ports were installed at heights of 2.5, 13.0, and 34.5 cm from the bottom, and, respectively, corresponded to the bottom, middle, and top of the anaerobic sludge bed. As shown in Figure 5, the ISC modeling results match the measured tracer trajectories well.

As the number of CSTR and their volumes in the ISC model change with the varying operating conditions and reactor size, modeling at varied HRTs and reactor sizes is performed to explore the reactor mixing characteristics.

Biogas production might be an important reason for the mixed flow at a high hydraulic loading rate, which also corresponds to a high organic loading rate at a fixed influent substrate level. Because of a lower superficial liquid velocity, the biogas production rate has a much more significant effect on the flow patterns of the UASB reactor. In addition to the

Table 2. Parameter Estimation Results of the Two Models for the Laboratory-Scale H_2-Producing UASB Reactor

		HRT (h)			
Model	Parameter	4.3	8.0	16.3	26.4
ISC model	V_{eff} (l)	6.7	5.9	7.5	7.5
	N	3	4	3	2
	Volume ratio of tanks	1:1.5:4.2	1:2:5:6.75	0.6:1:5.9	1:4
	Final χ^2	25.8	38.0	6.9	9.4
EESC model	V_{eff} (l)	6.7	5.9	7.5	7.5
	N	2.1	2.1	1.7	1.9
	Final χ^2	45.6	131.4	40.9	26.2

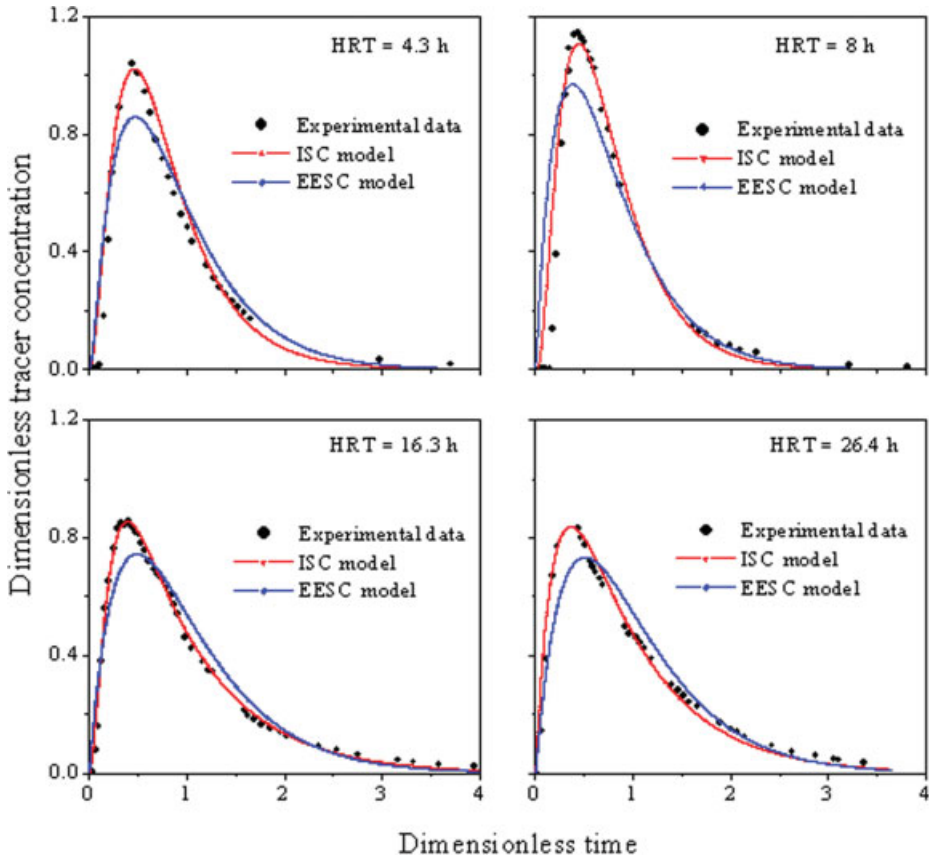

Figure 3. Simulated and measured tracer concentrations for the laboratory-scale H_2-producing UASB reactor effluent at various HRTs.

[Color figure can be viewed in the online issue, which is available at www.interscience.wiley.com.]

superficial liquid velocity, which is related to HRT, the superficial gas velocity is greatly dependent on the gas production rate and reactor size (i.e., cross section area). In our work, the two parameters, i.e., superficial gas and liquid velocities, are used to evaluate the simulated tracer trajectories for the six data sets (Table 3 and Figure 6a). The volume ratios of the last tank for data sets 1# and 2# are much greater than the others (Table 3). This implies that a signifi-

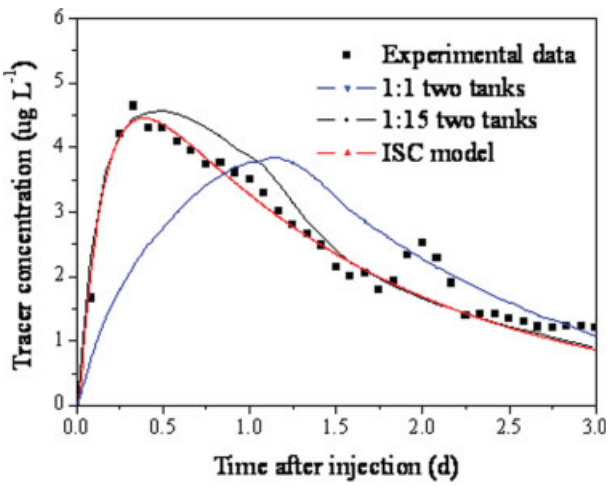

Figure 4. Simulated and measured tracer concentrations for the full-scale CH_4-producing UASB reactor effluent at an HRT of 24 h.

[Color figure can be viewed in the online issue, which is available at www.interscience.wiley.com.]

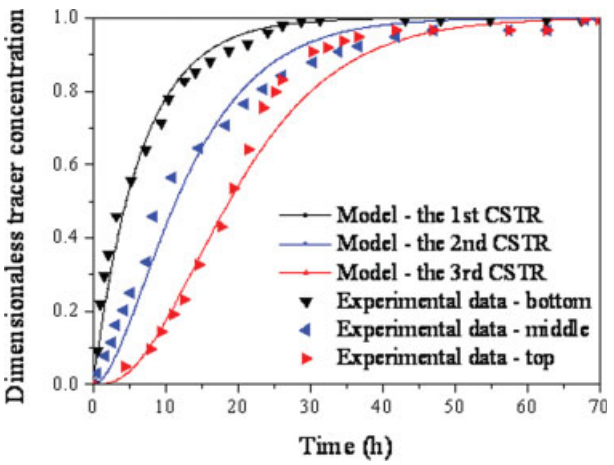

Figure 5. Simulated and measured tracer concentrations along the height of the laboratory-scale H_2-producing UASB reactor.

[Color figure can be viewed in the online issue, which is available at www.interscience.wiley.com.]

Table 3. Parameters Values Calculated with the ISC Model Under Different Operating Conditions

Experimental Set #	HRT (h)	u_g (m h^{-1})	u_l (m h^{-1})	N	Volume Ratio of Tanks
1	10.3	0.138	0.049	4	1:2.3:3.3:26.7
2	12.0	0.027	0.042	3	1:1.9:11.4
3	16.0	0.005	0.032	3	1:2.1:2.8
4	17.0	0.033	0.030	3	1:1.9:4.3
5	20.0	0.019	0.025	3	1:1.1:3.8
6	21.7	0.043	0.024	3	1:1.5:5.2

cant mixing is present in the reactor under the tested conditions. However, minor changes are observed for the number of tanks in the ISC model with the data sets in Table 3. This suggests that the steps of dispersion change along the UASB reactor height are of similar levels in most cases. The volume ratio is dependent heavily on the operating conditions. A higher superficial velocity results in a greater volume ratio of the last tank in the ISC model, and accordingly a more vigorous mixed flow pattern (Table 3).

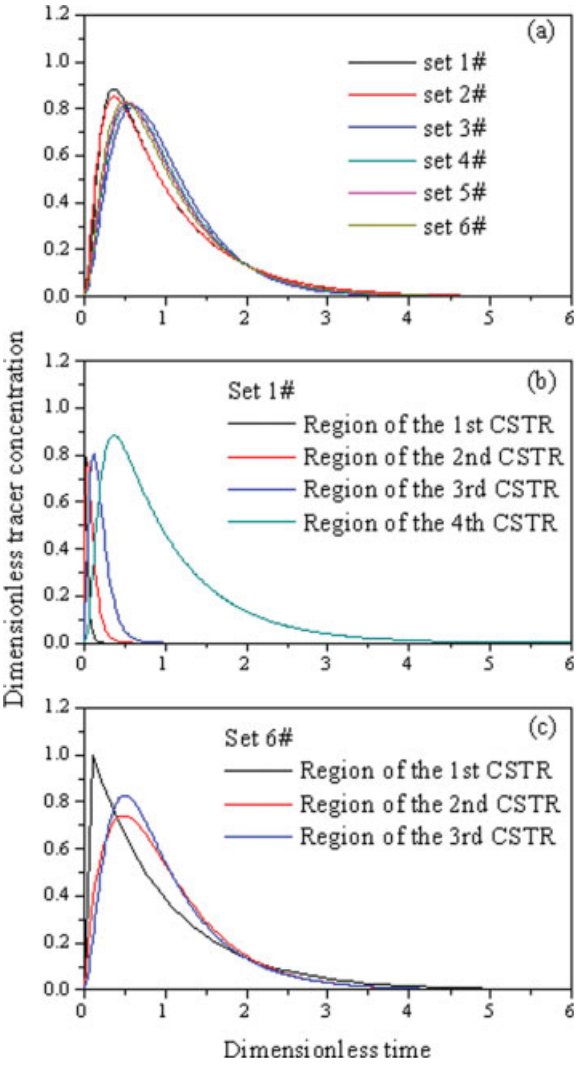

Figure 6. Modeling results under different operating conditions: (a) tracer concentrations of the reactor effluent for the six data sets; (b) tracer concentrations of each tank in the ISC model for the data set 1#; (c) tracer concentrations of each tank in the ISC model for the data set 6#.

[Color figure can be viewed in the online issue, which is available at www.interscience.wiley.com.]

The simulation results with the ISC model demonstrate the discontinuity in the mixing behavior throughout the UASB reactor. The tracer concentrations in each tank for the data sets 1# and 6# simulated with the ISC model are shown in Figures 6b,c, respectively, as an example. For the data set 6# with a low superficial velocity (Table 3), the time delay between the tracer trajectories at each tank is significant. On the other hand, for data set 1# with a higher superficial velocity, a minor time delay is observed (except the trajectory of the last tank), attributed to the near mixing flow patterns.

Flow pattern visualization

A structured numerical grid with a total number of 120,000 cells is implemented (Figure 7). The numerical simulation is carried out for transient conditions with a total time duration of 22 s. Figure 8 shows the solid phase holdup distribution in the UASB reactor. The sludge volume fraction decreases along the reactor height, similar to that reported previously.[11] Flow pattern simulation results are shown by the contours of velocity magnitude. The velocity magnitude increases with an increase in inlet flow velocity. However, the overall flow trends keep unchanged. Taking the laboratory-scale H_2-producing reactor as an example, the superficial velocities of liquid phase at an HRT of 4.3 h are visualized

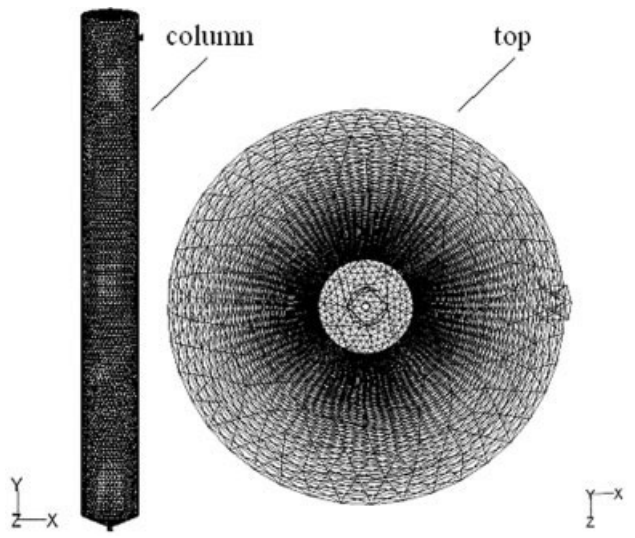

Figure 7. Mesh partition of the column and the top of the UASB reactor.

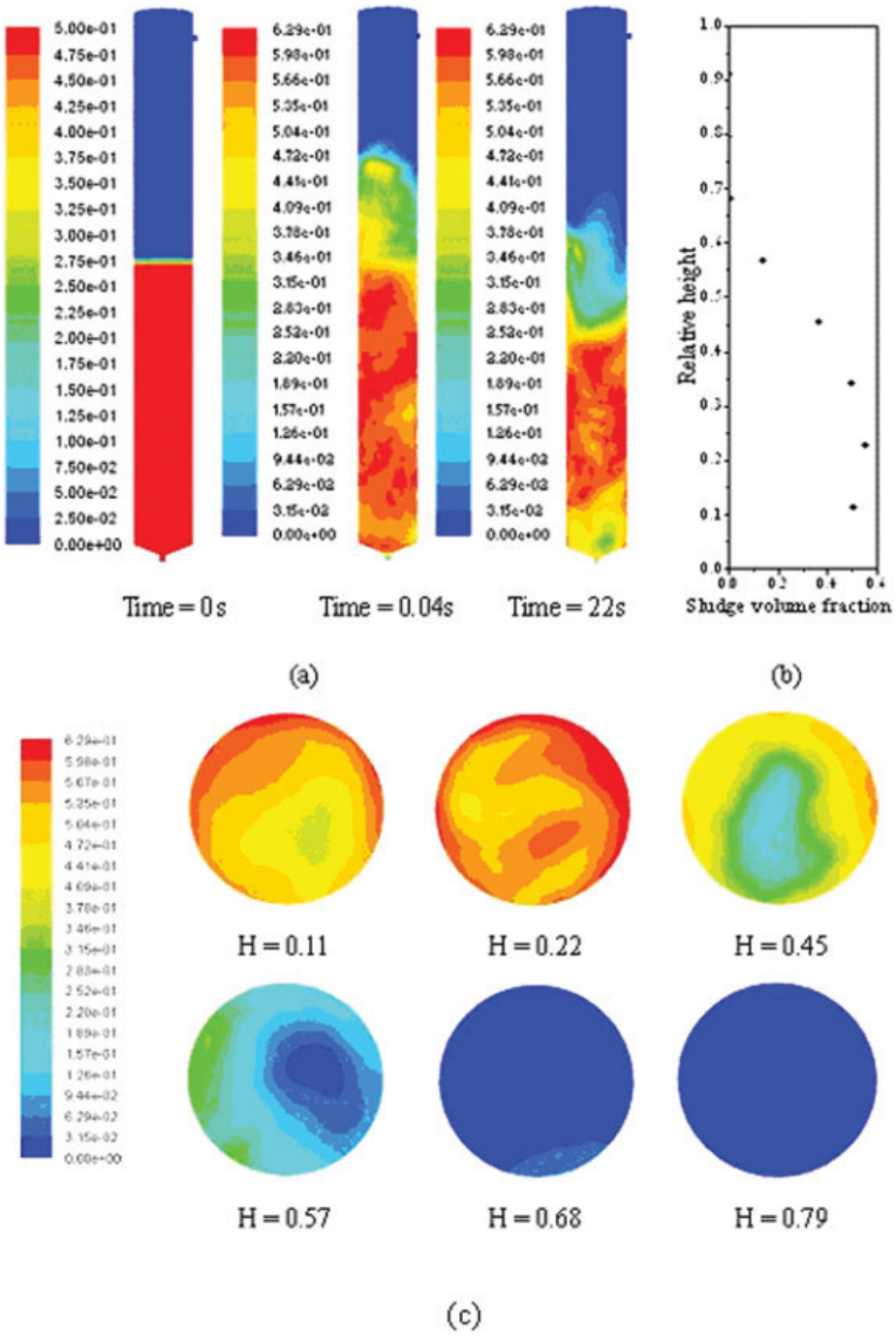

Figure 8. Transient model predictions of the laboratory-scale H_2-producing UASB reactor at an HRT of 4.3 h: (a) sludge volume fraction contours of sludge volume fraction at 0.11, 0.22, and 22 s; (b) average sludge volume fraction along the reactor height at 22 s; and (c) sludge volume fraction contours of sludge volume fraction of the reactor cross section at 22 s.

[Color figure can be viewed in the online issue, which is available at www.interscience.wiley.com.]

in Figure 9. The velocity magnitude scale can be referred to the magnitude bar at the left of each figure. The velocity magnitude increases along the UASB reactor height when the flow pattern is fully developed. Figure 10 shows that the superficial velocities of sludge phase are higher in the reactor bottom part and lower in the upper part. The flow field in Figures 9 and 10 further confirms the discontinuity in the mixing behavior throughout a UASB reactor, i.e., the dispersion decreases along the reactor axis from the bottom to the top.

Figure 11 shows the simulation of the gas accumulation in the sludge bed. With the 3-D unsteady CFD model simulation, the transience of the gas flow pattern can be visualized. The simulation results suggest that the mechanisms of the

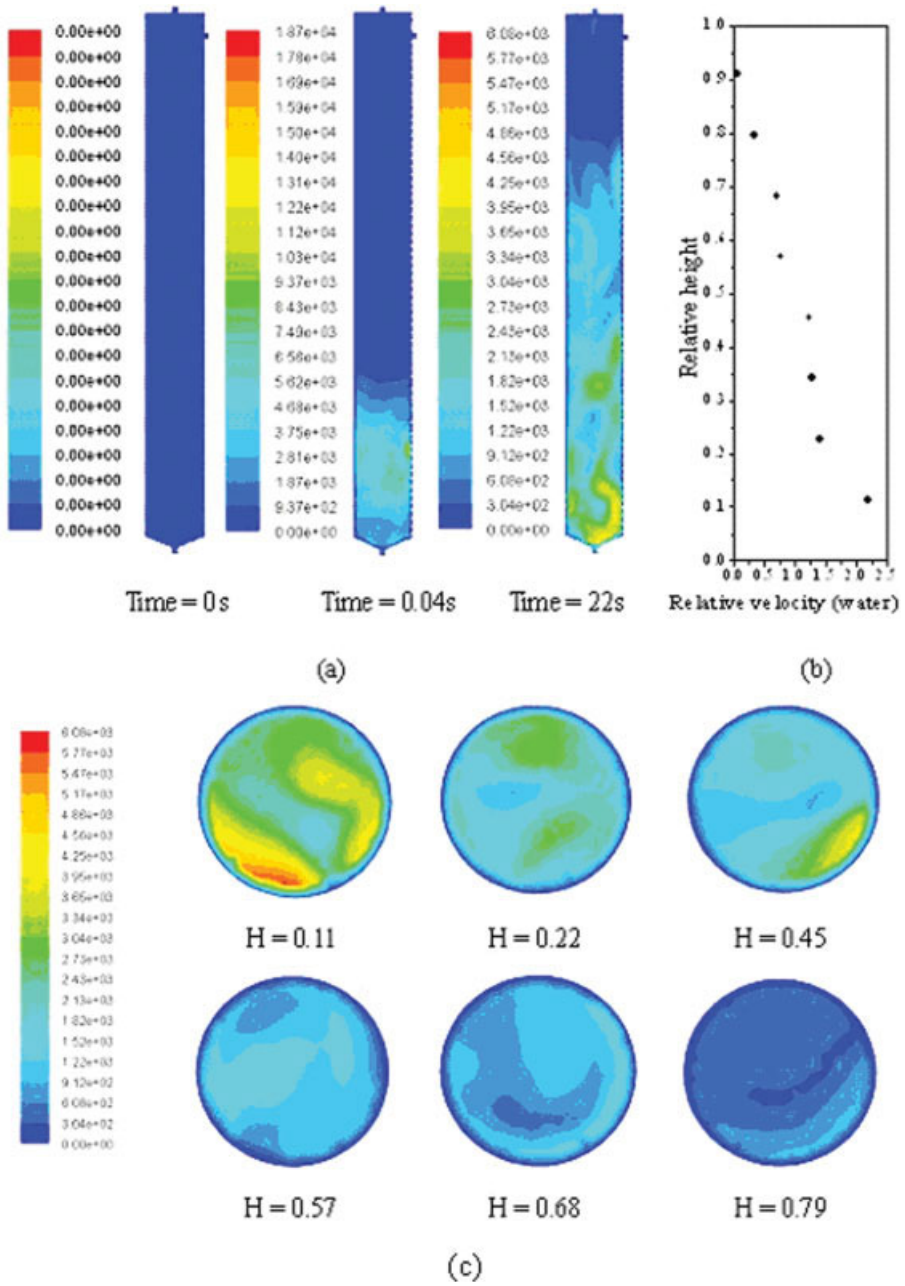

Figure 9. Transient model predictions of the laboratory-scale H_2-producing UASB reactor at an HRT of 4.3 h: (a) liquid velocity magnitude contours of liquid velocity magnitude at 0.11, 0.22 and 22 s; (b) average liquid relative velocity along the reactor height at 22 s; and (c) liquid velocity magnitude contours of liquid velocity magnitude of the reactor cross section at 22 s.

[Color figure can be viewed in the online issue, which is available at www.interscience.wiley.com.]

gas occasional abrupt release should be related to the force balance. When the force balance between gas and sludge is broken up, the gas release from the sludge bed will occur.

Discussion

Dispersion and flow patterns

The dispersion in a UASB reactor is significant. Compared with the EESC model, the ISC model is able to simulate the dispersion better. In the ISC model, the dispersion variations in a UASB reactor are emphasized through gradually increasing the size of tanks. This implies that the dispersion coefficient is reduced along the reactor axis and that its hydrodynamic behavior is basically dispersion-controlled.

There are several reasons responsible for the different dispersion coefficients between the sludge bed region and the blanket one. The size distribution and granule filling gradient are important factors, and they should result in a higher apparent linear superficial velocity and tighter packing in the sludge bed bottom than at the bed top or in the liquid zone

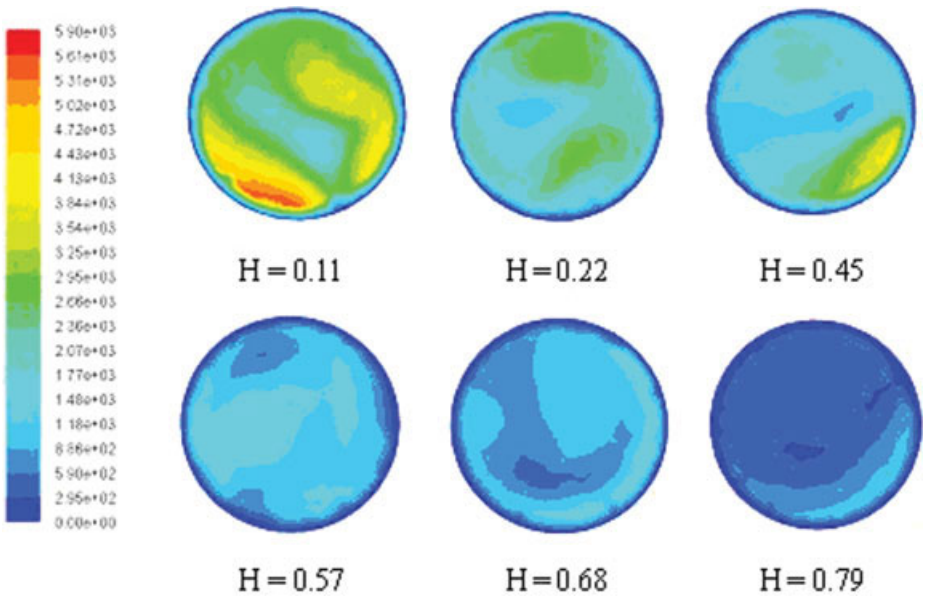

Figure 10. Contours of sludge velocity magnitude of the reactor cross section at 22 s.

[Color figure can be viewed in the online issue, which is available at www.interscience.wiley.com.]

(shown in Figures 8–10). Other important axial gradients, such as substrate, volatile fatty acids, and pH, are also significant factors. The dispersion in a UASB reactor cannot be adequately described by the ESC or EESC models because of the existence of significant gradients in substrate, volatile fatty acids, and pH. Their presence has a number of implications in process monitoring and controlling, especially in the dispersion analysis. As the importance of dispersion modeling in simulating UASB reactor hydrodynamics is demonstrated in this work, an agreement between the measured and simulated results is achieved using the ISC model.

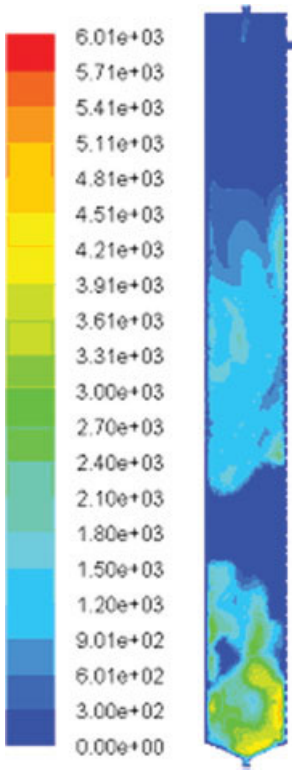

Figure 11. Visualized transience of the gas flow patterns in a UASB reactor at 22 s.

[Color figure can be viewed in the online issue, which is available at www.interscience.wiley.com.]

Moreover, the number of tanks (N) in the ISC model is calculated to be no more than four with the experimental results in Tables 2 and 3. This is attributed to the fact that the dispersion variation along the height of a UASB reactor is of similar levels in most cases. The 3-D CFD simulation results also show that the overall flow trends are similar under different hydraulic conditions.

The regions with low velocities are termed as stagnant or dead zones shown in Figures 9 and 10. The volume of the dead zones can be estimated by calculating the total volume of the cells with low superficial liquid velocities. The regions with the superficial liquid velocities less than 5% of the average velocity are considered to be stagnant or inactive regions. For this case, the dead or stagnant volume in the reactor is 10% of total reactor volume. This value is comparable with the results calculated with the ISC model as shown in Table 2.

Validity of the ISC model

The simulation results show that the ISC model is much better than the EESC model for describing the dispersion characteristics of UASB reactors (Figures 3 and 4). In the previous work by Batstone et al.,[27] although the ISC model was not established and applied, it was observed that the hydrodynamic behaviors of a full-scale CH_4-producing UASB reactor could be well simulated by a multi-CSTRs model concerning two-tank in series with a volume ratio of 1:15, rather than by a model regarding two-tank in series with a volume ratio of 1:1 (Figure 4). Results from both laboratory-scale H_2-producing and full-scale CH_4-producting

UASB reactors demonstrate that the ISC model is appropriate for describing the hydrodynamics of a UASB reactor, irrespective of that the reactor is laboratory- or full-scale, and that it is for H_2 or CH_4 production. Moreover, the RTD experimental data along the UASB reactor height (Figure 5) further demonstrate the validity of the ISC model. The results from the CFD simulation (Figures 8–10) are comparable with the ISC model predictions in terms of the similar flow patterns and the dead zone fractions. This suggests that these methods can be jointly used to explore the hydrodynamics of the UASB reactors.

As the effect of dispersion variation along the reactor axis is taken into account in the ISC model, the application of this model to systems with similar dispersion behaviors is expected. It is convenient to modify this model to adapt a new anaerobic wastewater treatment system. This hydrodynamic model might be also useful in simulating other bioreactors, such as fluidized bed reactor,[31] sequencing batch biofilm reactor[28] and packed-bed reactor.[32] Furthermore, through a combination of the hydrodynamics model with the biochemical kinetics and mass transfer models, a comprehensive model could be established to simulate the overall behaviors of anaerobic reactors, including reactor performance, sludge bed expansion and contraction, biogas accumulation and entrapment, biogas abrupt occasional release, granulation and degranulation process, granular sludge flotation, etc.

Conclusions

An ISC model was developed and successfully used to describe the hydrodynamics of UASB reactors. In such a model, a UASB reactor was visualized as being made-up of a number of CSTRs in series, and the dispersion coefficient decreases along the axis of the UASB reactor. As a result, its hydrodynamic behavior is basically dispersion-controlled. Experimental results from both laboratory-scale H_2-producing and full-scale CH_4-producing UASB reactors demonstrate that the ISC model established in this work was able to better describe the hydrodynamics of the UASB reactors than the other models. Moreover, a 3-D unsteady CFD model simulation was performed to visualize the phase holdup and obtain their flow patterns in a UASB reactor. The simulation results further confirm the discontinuity in the mixing behavior throughout the UASB reactor, i.e., the dispersion decreased along the reactor axis from bottom to top. These methods could be jointly used to elucidate the hydrodynamics of UASB reactors. The approach can be further used to design operate and optimize the UASB reactors. Furthermore, through a combination of a hydrodynamics model with biochemical kinetics and mass transfer models, a comprehensive model could be established for simulating the overall behaviors of anaerobic reactors.

Acknowledgments

The authors wish to thank the Natural Science Foundation of China (20577048, 50625825 and 50738006), the NSFC-JST Joint Project (20610002), and the National Basic Research Program of China (2004CB719602) for the partial support of this study.

Notation

C = tracer concentration, mg l^{-1}
$C(p)$ = calculated value of the model variable, mg l^{-1}
C_0 = initialize concentration in the 1st tank at $t = 0$ for the increasing-sized CSTRs model, mg l^{-1}
$C_{1,\varepsilon}$ = constant, dimensionless
$C_{2,\varepsilon}$ = constant, dimensionless
$C_{3,\varepsilon}$ = constant, dimensionless
C_D = drag coefficient, dimensionless
C_k = turbulent production, kg m^{-1} s^{-3}
C_L = lift coefficient, dimensionless
C_μ = constant, dimensionless
d = diameter, m
$E(t)$ = exit age distribution function, h^{-1}
$E(\theta)$ = dimensionless exit age distribution function, dimensionless
H = relative height, dimensionless
I_{in} = tracer loadings into the compartment, mg h^{-1}
k = turbulent kinetic energy, m^2 s^{-2}
k_{pl} = covariance of the velocities of the continuous phase and the dispersed phase, dimensionless
M = tracer mass, mg
M_D = drag force, N m^{-3}
M_I = interphase momentum transfer force, N m^{-3}
M_L = lift force, N m^{-3}
N = number of tanks in equal-sized CSTRs model
N_{time} = all sampling times
p = model evaluated parameters or pressure, dimensionless or Pa
Q = influent flow rate, m^3 h^{-1}
Q_{in} = discharge of water into the compartment, m^3 h^{-1}
r = volume fraction of a tank to the total volume of series tanks for the increasing-sized CSTRs model, dimensionless
Re = Reynolds number, dimensionless
t = time, h
$\bar{t}$ = average residence time, h
T = temperature, K
T_i = mean residence time in the single tank for the increasing-sized CSTRs model, h
u = superficial velocity, m h^{-1}
$\vec{u}_{pl}$ = relative velocity, m s^{-1}
$\vec{u}_{dr}$ = drift velocity, m s^{-1}
V_{tot} = total volume of all tanks for the increasing-sized CSTRs model, L

Greek letters

α = volume fraction, dimensionless
ε = dissipation rate, m s^{-3}
θ = dimensionless time, dimensionless
μ = viscosity accounting for turbulence, Pa s
μ_t = turbulent viscosity, Pa s
ρ = density, kg m^{-3}
σ = standard deviation, mg l^{-1}
σ_k = turbulent Prandtl numbers for k, dimensionless
σ_ε = turbulent Prandtl numbers for ε, dimensionless
σ_θ^2 = variance of the dimensionless residence time distribution, dimensionless
$\bar{\bar{\tau}}$ = stress tensor, Pa
χ^2 = squared difference between measured and calculated values of tracer concentrations at the sampling ports over all sampling times, dimensionless

Subscripts

eff = effective value
g = gas
i = i-th element of function
j = j-th element of function
k = physical quantity related to phase
l = liquid
N = quantities in the Nth compartment for the increasing-sized CSTRs model
s = solid

Superscripts

cal = calculated value
exp = measured value

Literature Cited

1. Pena MR, Mara DD, Avella GP. Dispersion and treatment performance analysis of an UASB reactor under different hydraulic loading rates. *Water Res*. 2006;40:445–452.
2. Heertjes PM, van der Meer RR. Dynamics of liquid flow in an upflow reactor used for anaerobic treatment of wastewater. *Biotechnol Bioeng*. 1978;20:1577–1594.
3. Heertjes PM, Kuijvenhoven LJ. Fluid flow pattern in upflow reactors for anaerobic treatment of beet sugar factory wastewater. *Biotechnol Bioeng*. 1982;24:443–459.
4. Bolle WL, van Breugel J, van Eybergen G, Kossen N, van Gils W. An integral dynamic model for the UASB reactor. *Biotechnol Bioeng*. 1986;28:1621–1636.
5. Costello DJ, Greenfield PF, Lee PL. Dynamic modeling of a single stage high-rate anaerobic reactor. II. Model verification. *Water Res*. 1991;25:859–871.
6. Martin AD. Interpretation of residence time distribution data. *Chem Eng Sci*. 2000;55:5907–5917.
7. Levenspiel O. *Chemical Reaction Engineering*, 3rd ed. New York: Wiley, 1999.
8. Brenner H. The diffusion model of longitudinal mixing in beds of finite length. *Chem Eng Sci*. 1962;17:229–237.
9. Singhal A, Gomes J, Praveen VV, Ramachandran KB. Axial dispersion model for upflow anaerobic sludge blanket reactors. *Biotechnol Prog*. 1998;14:645–648.
10. Makinia J, Wells SA. Evaluation of empirical formulae for estimation of the longitudinal dispersion in activated sludge reactors. *Water Res*. 2005;39:1533–1542.
11. Zeng Y, Mu SJ, Lou SJ, Tartakovsky B, Guiot SR, Wu P. Hydraulic modeling and axial dispersion analysis of UASB reactor. *Biochem Eng J*. 2005;25:113–123.
12. Kalyuzhnyi S, Fedorovich V, Lens P. Dispersed plug flow model for UASB reactors focusing on sludge dynamics. *J Ind Microb Biotech*. 2006;33:221–237.
13. Schmidt JE, Ahring BK. Granular sludge formation in upflow anaerobic sludge blanket (UASB) reactors. *Biotechnol Bioeng*. 1996;49:229–246.
14. Monahan SM, Vitankar VS, Fox RO. CFD predictions for flow-regime transitions in bubble columns. *AIChE J*. 2005;51:1897–1923.
15. Delnoij E, Kuipers JAM, van Swaaij WPM. Computational fluid dynamics applied to gas-liquid contactors. *Chem Eng Sci*. 1997;52:3623–3638.
16. Lapin A, Lübert A. Numerical simulation of the dynamics of two phase gas-liquid flows in bubble columns reactors. *Chem Eng Sci*. 1994;49:3661–3674.
17. Sokolichin A, Eigenberger G. Gas-liquid flow in bubble columns and loop reactors, Part 1: detailed modeling and numerical simulation. *Chem Eng Sci*. 1994;49:5735–5746.
18. Sokolichin A, Eigenberger G, Lapin A, Lübert A. Dynamic numerical simulation of gas-liquid two-phase flows: Euler/Euler versus Euler/Lagrange. *Chem Eng Sci*. 1997;52:611–626.
19. Pan Y, Dudukovic MP, Chang M. Numerical investigation of gas driven flow in 2D bubble columns. *AIChE J*. 2000;46:434–449.
20. Vesvikar MS, Al-Dahhan MH. Flow pattern visualization in a mimic anaerobic digester using CFD. *Biotechnol Bioeng*. 2005;89(6):719–732.
21. Wu BX, Chen SL. CFD simulation of non-Newtonian fluid flow in anaerobic digesters. *Biotechnol Bioeng*. 2008;99:700–711.
22. Reichert P. AQUASIM—a tool for simulation and data analysis of aquatic systems. *Water Sci Technol*. 1994;30:21–30.
23. Díez L, Zima BE, Kowalczyk W, Delgado A. Investigation of multiphase flow in sequencing batch reactor (SBR) by means of hybrid methods. *Chem Eng Sci*. 2007;62:1803–1813.
24. Mu Y, Yu HQ. Biological hydrogen production in a UASB reactor with granules. I. Physicochemical characteristics of hydrogen-producing granules. *Biotechnol Bioeng*. 2006;94:980–985.
25. Oh SE, van Ginkel S, Logan BE. The relative effectiveness of pH control and heat treatment for enhancing biohydrogen gas production. *Environ Sci Technol*. 2003;37:5186–5190.
26. APHA. *Standard Methods for the Examination of Water and Wastewater*, 19th ed. New York: American Public Health Association, 1995.
27. Batstone DJ, Hernandez JLA, Schmidt JE. Hydraulics of laboratory and full-scale upflow anaerobic sludge blanket (UASB) reactors. *Biotechnol Bioeng*. 2005;91:387–391.
28. Di Iaconi C, Ramadori R, Lopez A, Passino R. Hydraulic shear stress calculation in a sequencing batch biofilm reactor with granular biomass. *Environ Sci Technol*. 2005;39:889–894.
29. Yu HQ, Mu Y. Biological hydrogen production in a UASB reactor with granules II: reactor performance in 3-year operation. *Biotechnol Bioeng*. 2006;94:988–995.
30. Lou SJ, Tartakovsky B, Zeng Y, Wu P, Guiot SR. Fluorescence-based monitoring of tracer and substrate distribution in an UASB reactor. *Chemosphere*. 2006;65:1212–1220.
31. Asif M, Kalogerakis N, Behie L. Hydrodynamics of liquid fluidized beds including the distributor region. *Chem Eng Sci*. 1992;47:4155–4166.
32. van Zessen E, Tramper J, Rinzema A, Beeftink HH. Fluidized-bed and packed-bed characteristics of gel beads. *Chem Eng J*. 2005;115:103–1.

Manuscript received Jan. 25, 2008, revision received Jun. 18, 2008, and final revision received Aug. 19, 2008.